

Biodistribution of $^{68/67}\text{Ga}$ -Radiolabeled Sphingolipid Nanoemulsions by PET and SPECT Imaging

Sandra Díez-Villares ¹⁻³

Juan Pellico ^{4,5}

Noemí Gómez-Lado ⁶

Santiago Grijalvo ^{7,8}

Sandra Alijas¹

Ramon Eritja ^{7,8}

Fernando Herranz ^{5,9}

Pablo Aguiar ⁶

María de la Fuente ^{1,2}

¹Nano-Oncology and Translational Therapeutics group, Health Research Institute of Santiago de Compostela (IDIS), SERGAS, Santiago de Compostela, 15706, Spain; ²Biomedical Research Networking Center on Oncology (CIBERONC), Madrid, 28029, Spain; ³University of Santiago de Compostela (USC), Santiago de Compostela, 15782, Spain; ⁴School of Biomedical Engineering & Imaging Sciences, King's College London, St. Thomas' Hospital, London, SE1 7EH, UK; ⁵Biomedical Research Networking Center on Respiratory Diseases (CIBERES), Madrid, 28029, Spain; ⁶Nuclear Medicine Department and Molecular Imaging Group, Health Research Institute of Santiago de Compostela (IDIS), SERGAS, Santiago de Compostela, 15706, Spain; ⁷Institute for Advanced Chemistry of Catalonia (IQAC), Consejo Superior de Investigaciones Científicas (CSIC), Barcelona, E-08034, Spain; ⁸Biomedical Research Networking Center on Bioengineering, Biomaterials and Nanomedicine (CIBER-BBN), Madrid, 28029, Spain; ⁹NanoMedMol Group, Instituto de Química Médica (IQM), Consejo Superior de Investigaciones Científicas (CSIC), Madrid, 28006, Spain

Background and Purpose: Non-invasive imaging methodologies, especially nuclear imaging techniques, have undergone an extraordinary development over the last years. Interest in the development of innovative tracers has prompted the emergence of new nanomaterials with a focus on nuclear imaging and therapeutical applications. Among others, organic nanoparticles are of the highest interest due to their translational potential related to their biocompatibility and biodegradability. Our group has developed a promising new type of biocompatible nanomaterials, sphingomyelin nanoemulsions (SNs). The aim of this study is to explore the potential of SNs for nuclear imaging applications.

Methods: Ready-to-label SNs were prepared by a one-step method using lipid derivative chelators and characterized in terms of their physicochemical properties. Stability was assessed under storage and after incubation with human serum. Chelator-functionalized SNs were radiolabeled with ^{67}Ga and ^{68}Ga , and the radiochemical yield (RCY), radiochemical purity (RCP) and radiochemical stability (RCS) were determined. Finally, the biodistribution of $^{67/68}\text{Ga}$ -SNs was evaluated in vivo and ex vivo.

Results: Here, we describe a simple and mild one-step method for fast and efficient radiolabeling of SNs with ^{68}Ga and ^{67}Ga radioisotopes. In vivo experiments showed that $^{67/68}\text{Ga}$ -SNs can efficiently and indistinctly be followed up by PET and SPECT. Additionally, we proved that the biodistribution of the $^{67/68}\text{Ga}$ -SNs can be conveniently modulated by modifying the surface properties of different hydrophilic polymers, and therefore the formulation can be further adapted to the specific requirements of different biomedical applications.

Conclusion: This work supports $^{67/68}\text{Ga}$ -SNs as a novel probe for nuclear imaging with tunable biodistribution and with great potential for the future development of nanotheranostics.

Keywords: sphingomyelin nanoemulsions, biodistribution, gallium-68/67, nuclear imaging, nanotheranostics

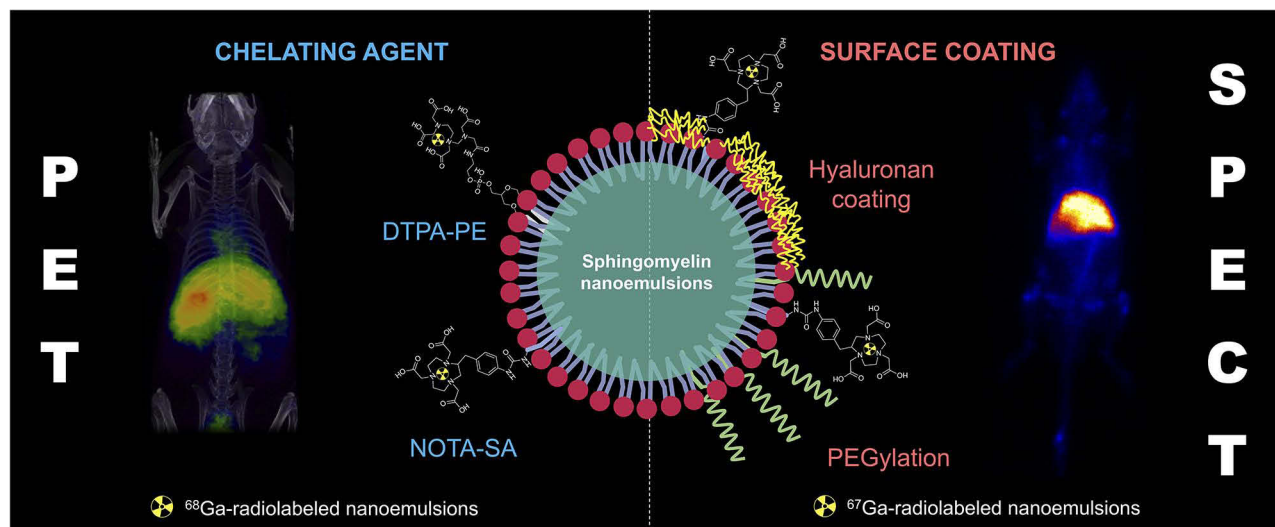
Introduction

Over the last decades, personalized medicine has greatly evolved with the development of imaging tools that improve the management of several diseases, especially cancer.¹ Among all the non-invasive imaging techniques, the nuclear imaging modalities Single Photon Emission Computed Tomography (SPECT) and Positron Emission Tomography (PET) stand out mainly due to their high sensitivity prospect of obtaining quantitative information. In fact, PET and SPECT imaging can provide detailed information about the in vivo behavior and pharmacokinetics of several compounds, such as nanomedicines, and can facilitate their translation to clinics.²

Correspondence: María de la Fuente Nano-Oncology Unit and Translational Therapeutics Unit, Health Research Institute of Santiago de Compostela (IDIS), Clinical University Hospital (CHUS), Building C, Floor -2, Lab 18, Travesía da Choupana s/n, Santiago de Compostela, ES15706, Spain Tel +34 981 955 704 Email maria.de.la.fuente.freire@sergas.es



Graphical Abstract



On the other hand, nanomedicine has emerged as a promising strategy to improve diagnosis and treatment of prevalent diseases including cancer.^{3,4} One of the most promising advantages of nanomedicine is the possibility to combine therapeutic molecules with diagnostic agents into single multifunctional nanoparticles, known as nanotheranostics, opening an entirely new field of development towards the implementation of personalized medicine.^{5,6} In recent years, the combination of nanoparticles with radionuclides is rapidly growing and there are a great number of submissions for the Food and Drug Administration approval.⁷ Different types of nanoparticles are investigated for nuclear medicine applications and multimodal imaging.⁸ For example, inorganic nanoparticles have been widely studied due to their intrinsic physical properties, that convert them into materials with a high potential for multimodal imaging.^{9,10} Nevertheless, organic nanoparticles are still the most in demand for the development of imaging probes by virtue of their biodegradable and biocompatible composition, preventing a long-term accumulation in the body and undesirable toxic side effects.¹¹ Indeed, liposomes are the most extended type of organic nanoparticles for nuclear imaging applications. Liposomes can be radiolabeled by different methodologies, which can be adapted to different kinds of nanoparticles, such as micelles, solid lipid nanoparticles, and nanoemulsions.¹² Chelator-based radiolabeling strategies offer a high versatility for the incorporation of radionuclides with different properties, suitable for complementary imaging techniques and nanotheranostics.¹³

Nanoemulsions are defined as nanoscale droplets in which two immiscible liquids are mixed to form a single phase. Their biocompatible composition, easy production by soft and scalable methodologies and improved drug loading capacity compared to liposomes, are relevant advantages that have prompted their use in biomedicine.^{14,15}

Nanoemulsions have been widely studied for fluorescence, MRI and ultrasounds imaging.^{16,17} However, their use in nuclear imaging is still recent and there are only few reports describing radiolabeled nanoemulsions.^{18–20} Our group has recently reported the development and characterization of sphingomyelin nanoemulsions that incorporate sphingomyelin, one of the main lipids in cell membranes (SNs), and claimed their potential in drug delivery.²¹ The principal advantages of SNs relate to their safe and simple composition, long-term colloidal stability, and capacity for accommodation of different types of functionalities and therapeutic payloads.^{21–23} Previous attempts by our research group have proved that SNs can be radiolabeled with Fluorine-18 for PET imaging following a maleimide reaction. However, radiochemical yields (RCY) were found to be highly dependent on the crosslinking efficacy.²⁴ The aim of this work was to provide an optimized composition and straightforward methodology for the radiolabeling of SNs with ^{68}Ga and ^{67}Ga radioisotopes using a chelator-based strategy. Radiolabeled formulations can be used for indistinct application in PET and SPECT imaging, and therefore adaptable to specific needs and biomedical applications.

Materials and Methods

Synthesis and Characterization of NOTA-Stearylamine Derivative

Octadecylamine (stearylamine, >99%, Merck Group, Darmstadt, Germany) was conjugated to 2-(4-isothiocyanatobenzyl)-1,4,7-triazacyclononane-1,4,7-triacetic acid (*p*-SCN-Bn-NOTA, NOTA, >94%, Macrocylics, Dallas, TX, USA) to obtain a lipid derivative chelator for further inclusion into the nanoemulsions. Details about the reaction protocol and the product characterization are included in the [Supporting Information](#).

Preparation of Sphingomyelin Nanoemulsions

SNs were prepared following a method previously reported by our group with minor modifications.²¹ Briefly, oleic acid (5 mg, 65–88%, Merck Group, Darmstadt, Germany), egg sphingomyelin (0.5 mg, 98%, Lipoid GmbH, Ludwigshafen, Germany) and the surfactant C16/C18-COO-C₉H₉O₃ (0.5 mg, 96%, GalChimia S.L., A Coruña, Spain) with a lipid ratio 1:0.1:0.1 w/w were dissolved in 100 µL of absolute ethanol (99.7%, Cienytech S.L., A Coruña, Spain). All the additional lipid derivatives used to functionalize SNs, such as 1,2-dimyristoyl-*sn*-glycero-3-phosphoethanolamine-*N*-diethylenetriaminepentaacetic acid (DTPA, 0.05 mg, >99%, Avanti Polar Lipids, Alabama, AL, USA), NOTA (0.05 mg) or an oleic acid modified polyethylene glycol (PEG, 2 kDa, 0.125 mg, Nanocs, New York, NY, USA) were included in the organic phase. Then, this organic phase was injected in 1 mL of MilliQ water (Millipore Milli-Q system) under magnetic stirring using an insulin syringe (0.5 mL, 0.33 × 12 mm ICO.C.1) and nanoemulsions (SNs, DTPA-SNs, NOTA-SNs or NOTA-PEG-SNs) were spontaneously formed. To prepare SNs coated with hyaluronic acid (NOTA-HA-SNs), the organic phase containing the lipids and NOTA was injected under stirring in 1 mL of an aqueous solution of sodium hyaluronate (HA, 170 kDa, 2 mg mL⁻¹, >95%, Bioiberica, S.A.U, Barcelona, Spain).

Physicochemical and Morphological Characterization

All the nanoemulsions were physicochemically characterized using a Nanosizer 2000[®] (Malvern Instruments,

Malvern, UK). The mean size and its distribution, defined by the polydispersity index (PDI), were measured by Dynamic Light Scattering (DLS). Measurements were performed on disposable microcuvettes (ZEN0040, Malvern Instruments) upon dilution of the SNs in MilliQ water, reaching a final lipid concentration of 0.5 mg mL⁻¹. The zeta potential (ZP) was analyzed by Laser Doppler Anemometry (LDA) diluting SNs in MilliQ water (lipid concentration 0.12 mg mL⁻¹) with Folded capillary cuvettes (DTS1070, Malvern Instruments). The stability of SNs, DTPA-SNs and NOTA-SNs was tested under storage conditions at 4 °C up to one month and also after incubation with human serum at 37 °C for 72 h. The colloidal properties were measured by DLS maintaining the conditions mentioned before. Parameters such as the medium (water) and the temperature (25 °C) were fixed for all the measurements.

The morphology of SNs was observed by Field Emission Scanning Electron Microscopy (FESEM) using a ZEISS FESEM ULTRA Plus, microscope (Carl Zeiss Micro Imaging, GmbH, Germany). Before the measurement, 20 µL of sphingomyelin nanoemulsions (0.5 mg mL⁻¹) were stained with 20 µL phosphotungstic acid (2% w/v). Then, 20 µL of the mixture was placed on a carbon coated grid and left for 2 minutes. The excess was removed using a filter paper and the grid was allowed to dry. The grid was washed 5 times with 100 µL of filtered MilliQ water and it was dried overnight.

Cell Culture Conditions

A549 (ATCC[®] CCL-185), MDA-MB-231 (ATCC[®] HTB-26) were cultured in Dulbecco's modified Eagle's medium high glucose (DMEM, Merck Group, Darmstadt, Germany) and OMM-2.5 (kindly provided by Martine J. Jager from Leiden University Medical Center, Leiden, The Netherlands) were grown in RPMI (Gibco, Thermo Scientific S.L., Waltham, MA, United States). Both media were supplemented with 10% fetal bovine serum (FBS) and 1% penicillin:streptomycin (Gibco, Thermo Scientific S.L., Waltham, MA, United States). Cells were maintained at 37 °C with 95% relative humidity and 5% CO₂.

Cellular Uptake of SNs

Cellular uptake of SNs was studied by confocal microscopy. 8 × 10⁴ cells/well were seeded in an 8-well µ-chamber (SPL Life Sciences Co., Ltd., Gyeonggi-do, Korea). After 24 h, cells were treated with SNs (0.13 mg mL⁻¹ per well) labeled with C11-TopFluor sphingomyelin (>99%,

Avanti Polar Lipids, Alabama, Al, USA). After 4 h of incubation at 37 °C, cells were washed with 1x phosphate buffer saline (PBS) twice and fixed with 4% paraformaldehyde for 15 min. Cells were then washed twice with 1x PBS and the cellular nuclei were counterstained with Hoechst 33,342 (Thermo Scientific S.L., Waltham, MA, United States) for 5 min. After washing, the slide was mounted with Mowiol (Merck Group, Darmstadt, Germany) and a coverslip. The samples were left to dry in the dark overnight at RT, following their storage at -20 °C, until taken for observation under a confocal microscope (Confocal Laser Microscope Leica SP8®).

Radiolabeling of DTPA-SNs and NOTA-SNs with ⁶⁸Ga

⁶⁸Ga ($t_{1/2} = 68$ min, $\beta^+ = 89\%$ and $EC = 11\%$) was obtained from a ⁶⁸Ge/⁶⁸Ga generator system (ITG Isotope Technologies Garching GmbH, Germany) in which ⁶⁸Ge ($t_{1/2} = 270$ d) was attached to a column based on an organic matrix generator. The ⁶⁸Ga was eluted with 4 mL of 0.05 M hydrochloric acid. Then, 500 μ L of DTPA-SNs or NOTA-SNs (13 mg mL⁻¹) were mixed with 500 μ L of 4-(2-hydroxyethyl)-1-piperazineethanesulfonic acid buffer (HEPES, 0.5 M, pH 5.05). The mixture was incubated with 1.5 mL of ⁶⁸Ga (≈ 300 MBq) at 30 °C for 30 min and purified by PD-10 columns. The incorporated radioactivity was measured in an activimeter (AtomLab™500, Biodex).

Radiolabeling of NOTA-SNs, NOTA-HA-SNs and NOTA-PEG-SNs with ⁶⁷Ga

⁶⁷Ga-citrate ($t_{1/2} = 78.3$ h, 100% $EC = 39\%$ γ 93 keV, 21% γ 185 keV, 17% γ 300 keV) was obtained from CURIUM (France) as sterile solution with a pH between 5 and 8 and a radiochemical purity at least equal to 95%. ⁶⁷Ga-citrate solution was converted to ⁶⁷GaCl₃ using a method previously described.²⁵ In brief, 2 mL of ⁶⁷Ga-citrate (37 MBq) diluted in distilled water was filtered with a SEP-PAK® Plus silica cartridge (ABX, Advanced Biochemical Compounds, Germany) using a 5 mL plastic syringe. Afterwards, the silica cartridge was washed three times with 5 mL of distilled water to remove the free citrate ions. The ⁶⁷Ga³⁺ ions were eluted with 3 mL of HCl 0.1 M, obtaining a solution of ⁶⁷GaCl₃ which was concentrated on a rotary vacuum evaporator to get a final volume of 500 μ L. The pH was adjusted to 4–5 with NaOH 0.1 M and the solution was incubated with 500 μ L of NOTA-SNs, NOTA-HA-SNs or NOTA-PEG-SNs (10 mg mL⁻¹) diluted in HEPES buffer (1.5

M, pH 5.05) for 1 h at 37 °C. The labeled nanoemulsions were eventually purified with PD-10 columns and the radioactivity was measured in the activimeter.

Radiochemical Characterization

The radiochemical yield (RCY) was calculated as a percentage of decay corrected activity found in the post-purification solution compared to the starting activity. The radiochemical stability (RCS) of ⁶⁸Ga-labeled nanoemulsions was assessed by incubating the emulsions with animal serum at 37 °C for 4 hours. In case of ⁶⁷Ga-labeled nanoemulsions, the stability was measured after incubation with animal serum for 0, 24, 48 and 72 h, according to the acquisition time points. In both cases, after the incubation time the mixture was purified by a PD-10 column and the activity of the elution was measured and decay corrected. Radiochemical purity (RCP) was analyzed by instant thin-layer chromatography (ITLC), and details regarding experimental protocols are included in the [Supporting Information](#).

In vivo Biodistribution by PET/CT and SPECT Imaging

In vivo PET/CT imaging was performed in healthy mice (C57BL/6) with a nanoPET/CT small-animal imaging system (Mediso Medical Imaging Systems, Budapest, Hungary). List-mode PET data acquisition commenced 2 hours post bolus injection of ~ 12 MBq of ⁶⁸Ga-DTPA-SNs or ⁶⁸Ga-NOTA-SNs (12 MBq, $n = 5$) through the tail vein and continued for 30 minutes. At the end of PET, microCT was performed for attenuation correction and anatomic reference. The dynamic PET images in a 105 \times 105 matrix (frame rates: 3 \times 10 min, 1 \times 30 min, 1 \times 60 min) were reconstructed using a Tera-Tomo 3D iterative algorithm. Acquisition and reconstruction were performed with proprietary Nucline software (Mediso, Budapest, Hungary). Qualitative Image analysis in mice was performed using Osirix software (Pixmeo, Switzerland). Animal experiments were conducted according to the ethical and animal welfare committee at CNIC and the Spanish and UE legislation. Experimental protocols have been approved by Madrid regional government (PROEX16/277).

SPECT studies were carried out on male Sprague-Dawley rats with an average weight of 299.5 ± 23.45 g supplied by the animal facility at the University of Santiago de Compostela (Spain). Planar dynamic SPECT images were acquired with a single-head clinical Siemens Orbiter gamma camera (Siemens Medical Solutions, Inc.,

USA) using a parallel collimator specifically designed for low-energy photons and high spatial resolution. Data were acquired in list-mode format in order to apply energy and spatial linearity, and uniformity corrections. In vivo NOTA-SNs and free ^{67}Ga biodistribution were studied after the intravenous injection (17.70 ± 8.5 MBq, $n = 5$) in healthy rats at different time-points: 24, 48 and 72 h. In order to compare the differences in biodistribution between NOTA-SNs, HA-SNs and PEG-SNs, healthy rats were intravenously injected (13.2 ± 0.3 MBq, $n = 3$) and the images were acquired dynamically during the first 60 min after injection (30 frames/2min). All images were analyzed using AMIDE software (amide.sourceforge.net). Quantitative analysis was carried out in a dynamic study by using circularly delineated Regions of Interest (ROIs) in the heart and liver, with 9 mm in diameter. The mean uptake was calculated over time in every region averaged over each of the 3 frames (6 min) and the results were reported as heart-to-liver ratio.

Ex vivo Biodistribution Studies

Ex vivo biodistribution of ^{68}Ga -labeled nanoemulsions was conducted 4 h post-injection. In case of ^{67}Ga -labeled nanoemulsions, biodistribution studies were performed 72 h post-injection. Animals were sacrificed in a CO_2 chamber, organs were extracted and counted with a Wizard 1470 gamma counter (Perkin Elmer) for 1 min each ($n=5$ per experiment). Radioactivity decay was corrected, and a biodistribution was presented as the percentage of injected dose per gram (% ID/g).

Statistical Analysis

All the experiments were performed at least in triplicate. Data are expressed as mean \pm standard deviation (SD). Statistical analyses were calculated using GraphPad Prism[®] software (version 8.0). Student's *t*-test was used to compare significant differences between the two groups. * ($p \leq 0.05$), ** ($p \leq 0.01$), *** ($p \leq 0.001$) was considered statistically significant.

Results and Discussion

Preparation and Characterization of SNs, DTPA-SNs and NOTA-SNs

Here, we describe the radiolabeling of SNs with Gallium-68 and Gallium-67 for their application in PET and SPECT imaging. SNs were prepared by ethanol injection, a one-step mild technique that allows obtaining colloidal nanoemulsions

within seconds (Figure 1A, left). The reproducibility of the preparation method (Figure 1A, right) was obtained after measuring 24 independent batches by DLS (raw data are showed in Table S1). SNs showed spherical morphology, as observed in FESEM images (Figure 1B). Additionally, SNs were efficiently internalized in cancer cells (Figure 1C), which is a relevant factor to take into account in order to determine the potential of a formulation for biomedicine applications. Stability determinations in cell culture media were also performed and are shown in Figure S1, Supporting Information. To convert SNs into suitable probes for PET and SPECT imaging, we followed a chelator-mediated approach, which is one of the most used methods to radiolabel nanoparticles with radionuclides, such as ^{64}Cu , ^{68}Ga , $^{99\text{m}}\text{Tc}$ or ^{111}In .^{13,26} Labeling organic nanoparticles, and especially lipid nanoparticles, can be done by the use of lipid-derivative chelators. These conjugates can be inserted into the membrane of the lipid particles at the time of their preparation.^{27–29} In this study, we used two different lipid-derivative chelators to determine the best candidate for in vivo imaging. First, we selected the acyclic chelator diethylenetriaminepentaacetic acid modified with a dimyristoyl-sn-glycero-3-phosphoethanolamine chain (DTPA). Second, we synthesized the amphiphilic derivative of the macrocyclic chelator 1,4,7-triazacyclononane-1,4,7-triacetic acid (NOTA) as previously described.^{30–32} In brief, a stearylamine was reacted with the isothiocyanate macrocycle *p*-SCN-Bn-NOTA (1, Figure S2A, Supporting Information). The nucleophilic substitution in *N,N*-dimethylformamide afforded the corresponding thiourea derivative (2, NOTA-stearylamine, Figure S2A, Supporting Information) after recrystallization at moderate yield (23%). The NOTA-stearylamine derivative 2 was characterized by high-resolution mass spectrometry (Figure S2B Supporting Information) and NMR, confirming its structure (Figures S3 and S4 Supporting Information). Both lipid-modified chelators were spontaneously incorporated into the lipidic layer of SNs. According to results shown in Table 1, a slight increase in size was observed for DTPA-SNs and NOTA-SNs with respect to the control SNs, which could be indicative of the efficient incorporation of the chelators. In all cases, we observed a narrow distribution of the particles with a PDI ≤ 0.2 .

Stability studies under storage conditions at 4 °C showed that all the formulations were highly stable during the tested period (Figure 2A), indicating that the incorporation of the lipid-derivative chelators does not compromise the colloidal properties of SNs. In addition, they showed high stability in the human serum for 72 h at 37 °C, as shown in Figure 2B, demonstrating their potential for

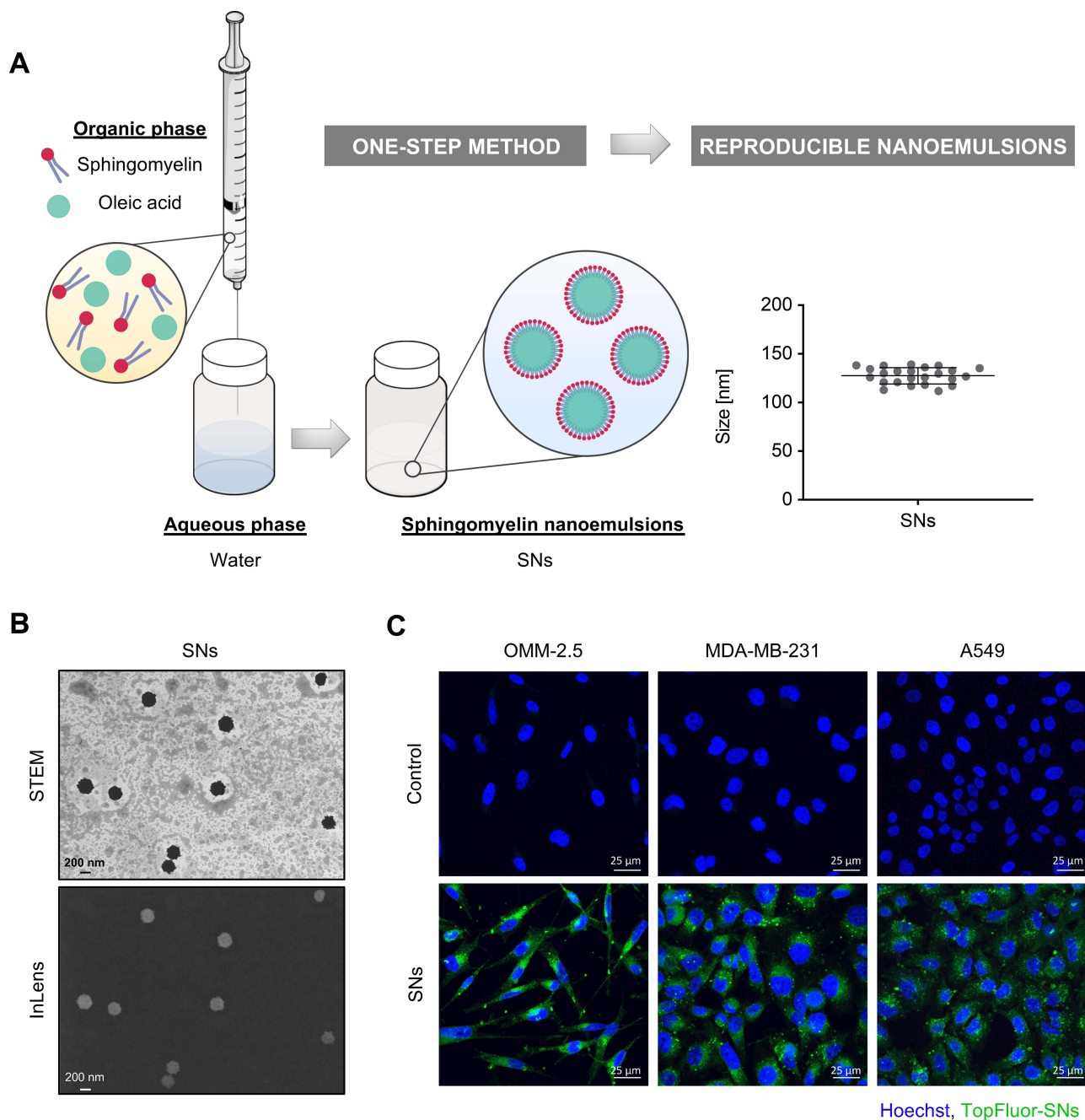


Figure 1 (A) Scheme of the one-step method used for the preparation of SNs (left) and the method reproducibility after measuring the hydrodynamic size of 24 independent batches by DLS (right); horizontal bars represent size mean and standard deviation (127 ± 9 nm). (B) Representative Field Emission Scanning Electron Microscopy (FESEM) images of SNs acquired with STEM (top) and InLens (bottom) detectors. (C) Confocal microscopy images showing the internalization of SNs in different cancer cell lines. SNs are labeled in green (TopFluor-SM) and cell nuclei are labeled in blue (Hoechst).

in vivo applications. Although organic nanoparticles offer relevant advantages with respect to inorganic nanoparticles, in general, their preparation is still complex, as dendrimers, liposomes or nanogels tend to require multi-step preparation methods and/or typically the use of high-energy techniques. On the contrary, this methodology provides long-term stable DTPA-SNs and NOTA-SNs particles in few

minutes through a one-step protocol. Moreover, the preparation of DTPA-SNs and NOTA-SNs avoids the use of high-energy techniques and uses low-cost and conventional starting materials. In fact, compared with previously reported organic nanosystems, we describe here the simplest and easiest methodology for the gallium radiolabeling through a chelator-based strategy.^{33–35}

Table 1 Physicochemical Characterization of SNs, DTPA-SNs and NOTA-SNs Measured by DLS and LDA (Results are Expressed as Mean \pm Standard Deviation, $n = 3$)

Formulation	Size [nm]	PDI	Zeta Potential [mV]
SNs	125 \pm 1	0.14 \pm 0.05	- 49 \pm 5
DTPA-SNs	136 \pm 3	0.20 \pm 0.02	- 51 \pm 3
NOTA-SNs	151 \pm 7	0.15 \pm 0.01	- 50 \pm 5

Abbreviation: PDI, polydispersity index.

Radiolabeling of DTPA-SNs and NOTA-SNs for PET Imaging

The combination of nanomaterials with ^{68}Ga for PET imaging has attracted a great deal of attention in recent years with several works devoted to the radiolabeling of inorganic nanoparticles.³⁶ However, only a few studies with organic nanoparticles, specifically PEGylated DTPA and NODAGA liposomes, PAMAM dendrimer-DOTA conjugates, NODAGA and DOTA nanogels, NODAGA polymeric nanoparticles and PSMA-DOTA microemulsions, have been reported so far.^{33,37–41}

DTPA-SNs, NOTA-SNs and non-chelator SNs (control) were radiolabeled by incubation with $^{68}\text{Ga}^{3+}$ at 30 °C for 30 min, and then purified by gel filtration in PD-10 columns. Figure 2C reveals that DTPA-SNs and NOTA-SNs were efficiently labeled with ^{68}Ga , reaching RCY of $82 \pm 4\%$ for DTPA-SNs and $92 \pm 2\%$ for NOTA-SNs. Differences in RCY might be related to some release of ^{68}Ga -DTPA-PE from the nanoemulsions in the purification process and/or to a better incorporation of the NOTA-SA derivative with SNs. With respect to the control formulation, nonspecific radiolabeling (RCY, $30 \pm 12\%$) was observed. This might be due to some entrapment of the radioisotope into the lipid membrane of the nanoemulsions mediated by electrostatic interactions. Radiochemical yields were in line with other works in the field, such as liposomes, nanogels, biopolymer nanoparticles and microemulsions.^{33,39–41} The radiochemical purity was evaluated by ITLC using a sodium citrate solution as mobile phase. Under these conditions, free ^{68}Ga showed a retention factor of 0.75 (Figure S5A, Supporting Information). In case of ^{68}Ga -nanoemulsions, we could not detect the presence of free ^{68}Ga , showing an RCP higher than 99% (Figure S5B, Supporting Information).

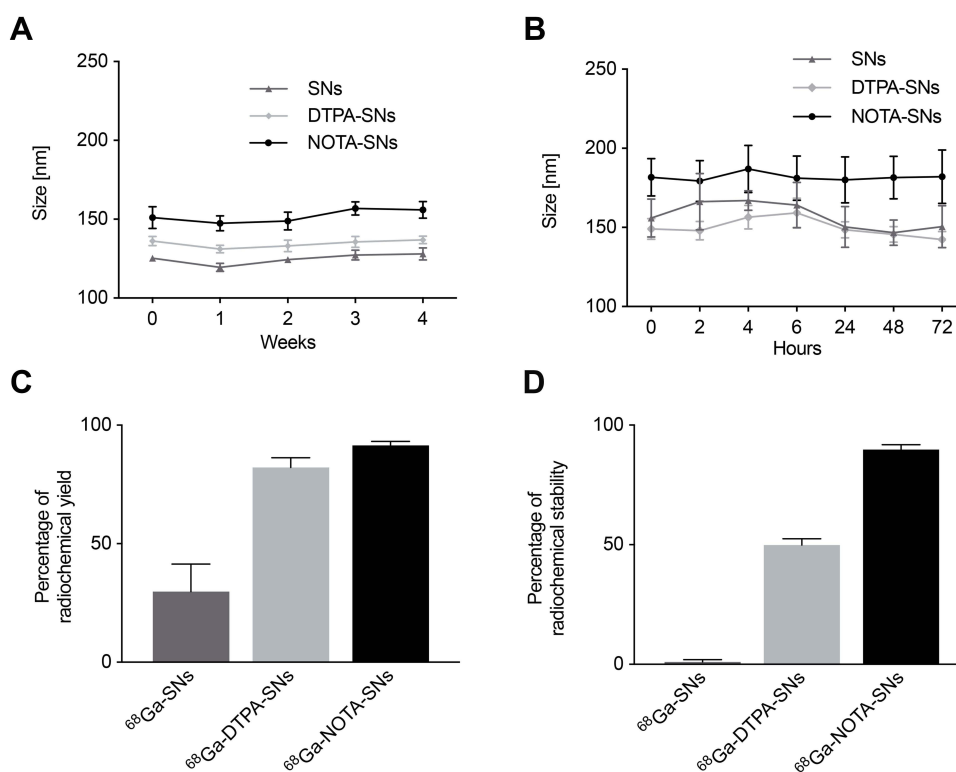


Figure 2 (A) Storage stability of SNs, DTPA-SNs and NOTA-SNs at 4 °C measuring the evolution of the average size by DLS for one month ($n=3$). (B) Stability in human serum at 37 °C during 72 h measured by DLS ($n=3$). (C) Radiochemical yield of ^{68}Ga -DTPA-SNs and ^{68}Ga -NOTA-SNs after incubation with the radioisotope for 30 min at 30 °C ($n=3$). (D) Radiochemical stability of ^{68}Ga -SNs, ^{68}Ga -DTPA-SNs and ^{68}Ga -NOTA-SNs after incubation with serum 4 h at 37 °C ($n=3$).

The RCS of the nanoemulsions upon incubation with serum at 37 °C was also determined (Figure 2D). As expected, radiolabeled control SNs (without a chelator) were not able to retain the gallium. In the case of DTPA-SNs, only $50 \pm 3\%$ of ^{68}Ga were retained, while NOTA-SNs showed the highest stability, retaining $90 \pm 2\%$ of activity, again in line with cyclic chelators as NODAGA or DOTA.^{37,39,40,42} On the other hand, although DTPA is commonly used to form complexes with gallium and other radioisotopes, the formation of less stable complexes can be a consequence of its acyclic structure.⁴³ This was confirmed after intravenous injection of DTPA-SNs and NOTA-SNs (12 MBq, n = 5) to healthy mice. 3D PET/CT images were acquired 2 h post-administration and showed major accumulation in the reticuloendothelial system (RES) organs and heart (Figure 3A). As expected, DTPA-SNs showed a higher circulation in the bloodstream due to the premature release of the radionuclide from the nanoemulsion. Ex vivo biodistribution results were conducted 4 h post-injection (Figure 3B) and corroborate major liver and spleen accumulation. This is in concordance with the in vivo pattern observed for most of the nanoparticles, especially lipid nanoparticles, such as liposomes and nanoemulsions.^{19,24,37,44} Remarkably, NOTA-SNs have a relatively long circulation time, showing a 10% of the injected dose in the bloodstream 4 h after intravenous injection. This in vivo pattern differs from other ^{68}Ga -labeled emulsions recently reported, with a shorter circulation half-life, mainly due to differences in size and composition.⁴¹ These results indicate that the pharmacokinetics of NOTA-SNs can be better studied after the radiolabeling with longer half-life radioisotopes, such as ^{67}Ga . Nevertheless, NOTA-SNs could be surface decorated with specific biomolecules in order to reduce their circulation time and to perform suitable probes for targeted ^{68}Ga molecular imaging.⁴⁵

Radiolabeling of NOTA-SNs with ^{67}Ga for SPECT Imaging

^{67}Ga , compared with ^{68}Ga ($t_{1/2} = 68$ minutes), allowed a long-term biodistribution study of NOTA-SNs by SPECT imaging. For NOTA-SNs radiolabeling, the clinical formulation ^{67}Ga -citrate was initially converted into the chloride form (GaCl_3) as previously described.²⁵ Briefly, ^{67}Ga -citrate was trapped in a silica cartridge, washed with distilled water and finally eluted with HCl 0.1 M, rendering a 90% yield. To ensure a successful

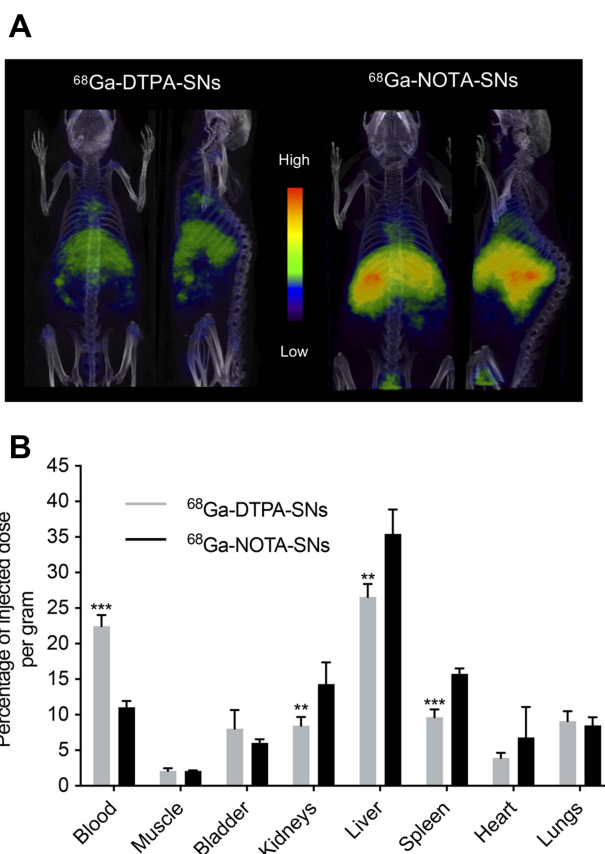


Figure 3 (A) Representative PET/CT whole-body coronal images of ^{68}Ga -DTPA-SNs and ^{68}Ga -NOTA-SNs biodistribution in healthy mice 2 h after intravenous injection (n=5). (B) Ex vivo biodistribution of both radiolabeled nanoemulsions 4 h post-injection (n=5). **($p \leq 0.01$), ***($p \leq 0.001$) was considered statistically significant.

radiolabeling and taking into account that with the half-life of ^{67}Ga there are no strong limitations for increasing the incubation time, we optimized the process (the solution was incubated with NOTA-SNs for 1 h at 37 °C). Then, the free radionuclide was removed by filtration in PD-10 columns, obtaining a $80 \pm 2\%$ of RCY (Figure 4A, before incubation with serum), between 10% and 20% higher than polymer and protein-based nanoparticles previously reported.^{34,46} The measured RCP was 98.9%, conducted by ITLC (Table S2, Supporting Information). In addition, RCS studies proved that the labeling was highly stable in serum over 72 h (Figure 4A). Then, due to the longer half-time of this radioisotope, SPECT studies were designed to evaluate the pharmacokinetics of NOTA-SNs at prolonged time periods. In vivo SPECT images were acquired 24, 48 and 72 h after intravenous injection of the radiolabeled NOTA-SNs. In parallel, we evaluated the in vivo uptake of the free radioisotope as a control. Animals injected with free ^{67}Ga (control) showed uptake in the bloodstream,

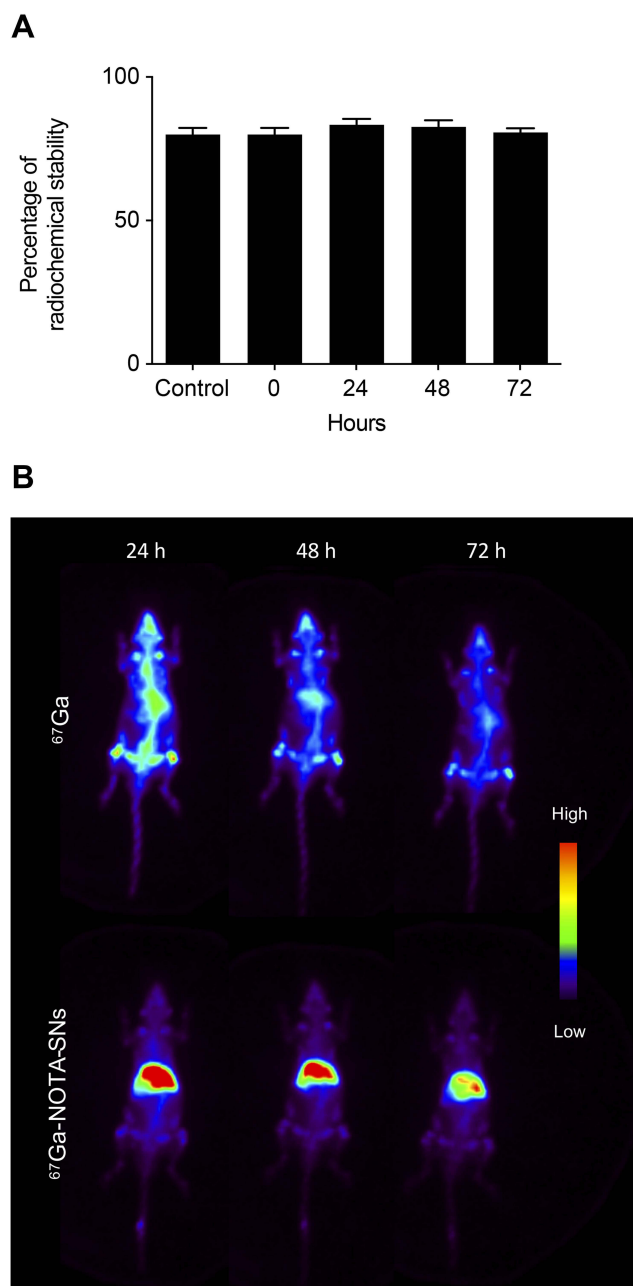


Figure 4 (A) Radiochemical yield of ^{67}Ga -NOTA-SNs (control) and radiochemical stability after incubation with serum 37 °C at different points (0, 24, 48 and 72 h, n=3). (B) Whole-body SPECT images showing the biodistribution of ^{67}Ga -NOTA-SNs compared with free ^{67}Ga during 72 h (n=5).

liver, lacrimal and salivary glands (Figure 4B), according previous reports.^{34,47} We can also observe free ^{67}Ga in the bladder and kidneys, a consequence of renal clearance. In comparison, NOTA-SNs showed similar biodistribution than observed in PET/CT images, with main accumulation in liver and RES organs, and its intensity decreases over time. After 72 h, we measured the ex vivo biodistribution and observed that the radioactivity remained only in liver

and spleen with less than 5% ID/g in both organs (Figure S6, Supporting Information). This could be related to the biodegradation of the particles and/or their excretion through the urine, in line with our previous report in which we described cationic fluorine-labeled nanoemulsions.²⁴ However, further studies must be carried out to determine the excretion routes of NOTA-SNs.

We finally investigated the possibility of surface-modification of NOTA-SNs without interfering with the radiolabeling procedure, to determine if it is possible to modulate the in vivo behavior.⁴⁸ Among the different strategies for surface modification that have been reported to date, PEGylation is the most established approach.⁴⁹ We coated NOTA-SNs with PEG (NOTA-PEG-SNs), using for this purpose a lipid-PEG derivative. However, it is well known that PEGylation might also lead to relevant drawbacks, such as the development of an immunological response, antibody generation and toxic side effects caused by the oxidative side products.⁵⁰ Bearing in mind these limitations, we have also investigated the in vivo effect of an alternative coating, hyaluronic acid (NOTA-HA-SNs). HA is a biocompatible polysaccharide widely used in biomedical research that has been reported to increase the circulating time of lipid nanoparticles.^{51,52} Surface-modified nanoemulsions (NOTA-PEG-SNs and NOTA-HA-SNs) presented a similar size than the reference formulation (NOTA-SNs) (Figure 5A). With respect to the zeta potential, relevant modifications were only noticed in the case of NOTA-HA-SNs, which rendered more negative values (Figure 5B). Radiolabeling with ^{67}Ga was successfully done, leading to RCY of $80 \pm 8\%$ and $76 \pm 1\%$ for NOTA-HA-SNs and NOTA-PEG-SNs, respectively (Figure 5C), indicating that the coatings do not significantly interfere in the interaction between the chelator and the radioisotope, and that coated NOTA-HA-SNs and NOTA-PEG-SNs could be tracked by SPECT in a comparable fashion to the reference formulation (NOTA-SNs) (Figure S7, Supporting Information).

A dynamic SPECT study was then carried out, and the tracer uptake ratio between heart and liver was calculated to evaluate the circulation/elimination pharmacokinetic profile. As shown in Figures 5E, ^{67}Ga -PEG-NOTA-SNs showed significantly higher circulation in the bloodstream in line with previous reports referring to PEGylated nanoemulsions.⁵³ Noteworthy, the PEGylation effect is observed even at a very low density (3 mol%), in concordance to other reports of nanoemulsions in which PEG densities vary between 0.5 and 50 mol% with respect to the total amount of

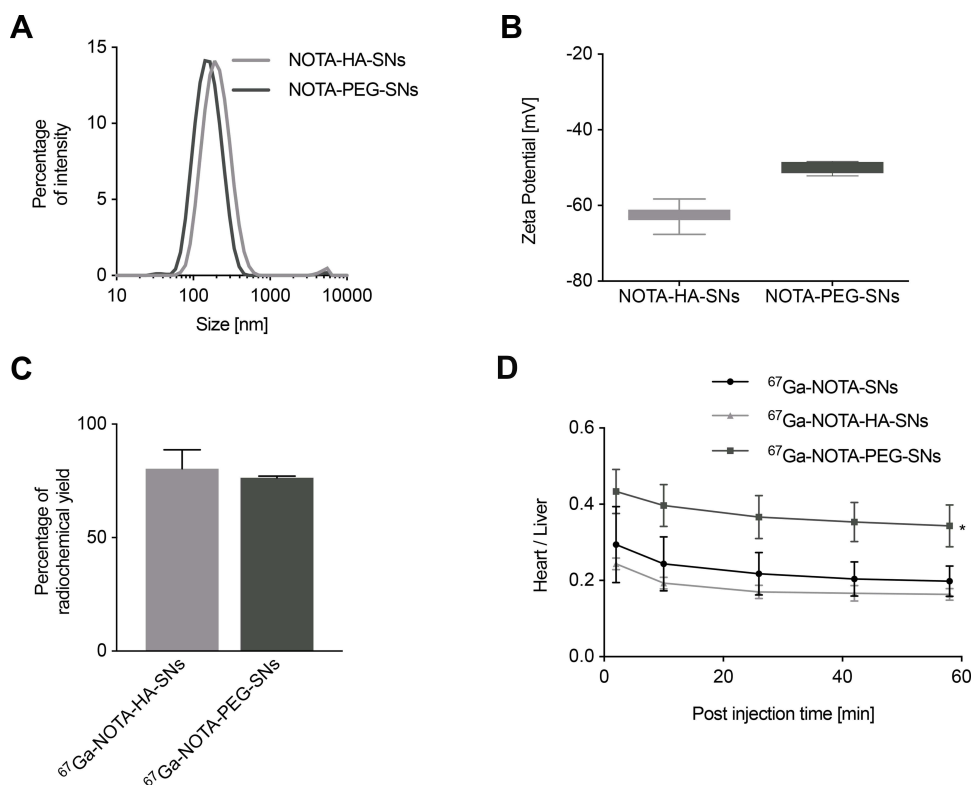


Figure 5 (A) NOTA-HA-SNs and NOTA-PEG-SNs hydrodynamic size distribution measured by DLS (171 ± 5 nm and 138 ± 8 nm, respectively, results are expressed as mean \pm standard deviation, $n=3$), (B) Zeta potential of NOTA-HA-SNs and NOTA-PEG-SNs measured by LDA (-64 ± 2 mV and -50 ± 1 mV respectively, results are expressed as mean \pm standard deviation, $n=3$). (C) Radiochemical yield of ^{67}Ga -NOTA-HA-SNs and ^{67}Ga -NOTA-PEG-SNs ($n=3$). (D) Quantitative analysis expressed as heart to liver ratio showing the differences in biodistribution between intravenously injected ^{67}Ga -nanoemulsions.

surfactant.^{53,54} In the case of NOTA-HA-SNs, the results were comparable to the reference formulation of NOTA-SNs, a fact that could be explained by the influence of the HA molecular weight and density of the coating. These factors will therefore need further optimization and will be the subject of future work intended for the development of applications in cancer nanotheranostics where HA coating could be particularly relevant to improve accumulation in the tumor.^{55,56} Altogether, these results confirm that it is possible to modulate the composition and in vivo behavior of NOTA-SNs, to open up their application in specific indications in the biomedical field.

Conclusion

We described here a simple and highly efficient preparation method for chelator-functionalized biocompatible SNs and the subsequent radiolabeling with ^{68}Ga and ^{67}Ga . The radiolabeled formulations showed great radiochemical properties for in vivo applications and were efficiently

followed-up by PET and SPECT imaging. Importantly, we have also proved that the biodistribution of the SNs can be modulated by modifying the surface properties. The capacity to modulate the radiolabeling, modality of imaging and tracking period, as well as the biodistribution properties, highlight the interest of SNs, which have the potential to be easily adapted to the requirements of different and specific biomedical applications. In summary, we believe that SNs have the potential for the development of advanced probes for nuclear imaging and nanotheranostics. In particular, future experiments could involve the evaluation of $^{68/67}\text{Ga}$ -SNs in tumor bearing animal models to further determine the real potential of this formulation in cancer nanotheranostics, taking into account the anticancer properties of ^{67}Ga .

Data Sharing Statement

All data generated or analyzed during this study are included in this published article and its [Supporting Information file](#).

Ethics Approval and Consent to Participate

Animal experiments were conducted according to the ethical and animal welfare committee at CNIC and the Spanish and EU legislation. Experimental protocols were approved by Madrid regional government (PROEX16/277).

Author Contributions

All authors contributed to data analysis, drafting or revising the article, have agreed on the journal to which the article will be submitted, gave final approval for the version to be published, and agreed to be accountable for all aspects of the work.

Funding

Authors thank the financial support given by Instituto de Salud Carlos III (ISCIII) and European Regional Development Fund (FEDER) (PI15/00828, PI18/00176 and DTS18/00133), by ERA-NET EURONANOMED III project METASTARG (AC18/00045) and by Asociación Española Contra el Cáncer (AECC, IDEAS18153DELA). The first author also acknowledges the financial support from Axencia Galega de Innovación (GAIN) and Xunta de Galicia (IN848C_20170721_7) and ISCII (FI19/00206).

Disclosure

The author reports no conflicts of interest in this work.

References

- Witney TH, Blower PJ. The chemical tool-kit for molecular imaging with radionuclides in the age of targeted and immune therapy. *Cancer Imaging*. 2021;21(1):1–14. doi:10.1186/s40644-021-00385-8
- Pérez-Medina C, Teunissen AJP, Kluza E, Mulder WJM, van der Meel R. Nuclear imaging approaches facilitating nanomedicine translation. *Adv Drug Deliv Rev*. 2020;154–155:123–141. doi:10.1016/j.addr.2020.07.017
- Gabizon AA, de Rosales RTM, La-beck NM. Translational considerations in nanomedicine: the oncology perspective. *Adv Drug Deliv Rev*. 2020;158:140–157. doi:10.1016/j.addr.2020.05.012
- Germain M, Caputo F, Metcalfe S, et al. Delivering the power of nanomedicine to patients today. *J Control Release*. 2020;326 (April):164–171. doi:10.1016/j.jconrel.2020.07.007
- Vázquez-Ríos AJ, Alonso-Nocelo M, Bouzo BL, Ruiz-Bañobre J, de la Fuente M. Nanotheranostics and their potential in the management of metastatic cancer. In: Conde J, editor. *Handbook of Nanomaterials for Cancer Theranostics*. Elsevier; 2018:199–244. doi:10.1016/b978-0-12-813339-2.00008-6
- Filippi L, Chiaravalloti A, Schillaci O, Cianni R, Bagni O. Theranostic approaches in nuclear medicine: current status and future prospects. *Expert Rev Med Devices*. 2020;17(4):331–343. doi:10.1080/17434440.2020.1741348
- Farzin L, Sheibani S, Moassesi ME, Shamsipur M. An overview of nanoscale radionuclides and radiolabeled nanomaterials commonly used for nuclear molecular imaging and therapeutic functions. *J Biomed Mater Res A*. 2019;107(1):251–285. doi:10.1002/jbm.a.36550
- Ge J, Zhang Q, Zeng J, Gu Z, Gao M. Radiolabeling nanomaterials for multimodality imaging: new insights into nuclear medicine and cancer diagnosis. *Biomaterials*. 2020;228. doi:10.1016/j.biomaterials.2019.119553
- Maccora D, Dini V, Battocchio C, et al. Gold nanoparticles and nanorods in nuclear medicine: a mini review. *Appl Sci*. 2019;9 (16):16. doi:10.3390/app9163232
- Venditti I. Engineered gold-based nanomaterials: morphologies and functionalities in biomedical applications. a mini review. *Bioengineering*. 2019;6(2):53. doi:10.3390/bioengineering6020053
- Mirahadi M, Ghanbarzadeh S, Ghorbani M, Gholizadeh A, Hamishehkar H. A review on the role of lipid-based nanoparticles in medical diagnosis and imaging. *Ther Deliv*. 2018;9(8):557–569. doi:10.4155/tde-2018-0020
- Man F, Gawne PJ, de Rosales RTM. Nuclear imaging of liposomal drug delivery systems: a critical review of radiolabelling methods and applications in nanomedicine. *Adv Drug Deliv Rev*. 2019;143:134–160. doi:10.1016/j.addr.2019.05.012
- Pellico J, Gawne PJ, de Rosales RTM. Radiolabelling of nanomaterials for medical imaging and therapy. *Chem Soc Rev*. 2021. doi:10.1039/d0cs00384k
- Singh Y, Meher JG, Raval K, et al. Nanoemulsion: concepts, development and applications in drug delivery. *J Control Release*. 2017;252:28–49. doi:10.1016/j.jconrel.2017.03.008
- Sánchez-López E, Guerra M, Dias-Ferreira J, et al. Current applications of nanoemulsions in cancer therapeutics. *Nanomaterials*. 2019;9 (6):6. doi:10.3390/nano9060821
- Anton N, Hallouard F, Attia MF, Vandamme TF. Nano-emulsions for drug delivery and biomedical imaging. In: Prokop A, Weissig V, editors. *Intracellular Delivery III, Fundamental Biomedical Technologies*. Springer. Vol. 8. 2016:273–300. doi:10.1007/978-3-319-43525-1_11
- Klymchenko AS, Liu F, Collot M, Anton N. Dye-loaded nanoemulsions: biomimetic fluorescent nanocarriers for bioimaging and nanomedicine. *Adv Healthc Mater*. 2021;10(1):1–27. doi:10.1002/adhm.202001289
- Wang C, Leach BI, Lister D, et al. Metallo-fluorocarbon nanoemulsion for inflammatory macrophage detection via PET and MRI. *J Nucl Med*. 2021;62(8):1146–1153. doi:10.2967/jnumed.120.255273
- Sofias AM, Toner YC, Meerwaldt AE, et al. Tumor targeting by $\alpha\beta$ -integrin-specific lipid nanoparticles occurs via phagocytosis hitchhiking. *ACS Nano*. 2020;14(7):7832–7846. doi:10.1021/acsnano.9b08693
- Navascuez M, Dupin D, Grande HJ, et al. COSAN-stabilised omega-3 oil-in-water nanoemulsions to prolong lung residence time for poorly water soluble drugs. *Chem Commun*. 2020;56 (63):8972–8975. doi:10.1039/d0cc00918k
- Bouzo BL, Calvelo M, Martín-Pastor M, García-Fandiño R, De La Fuente M. In vitro- in silico modeling approach to rationally designed simple and versatile drug delivery systems. *J Phys Chem B*. 2020;124 (28):5788–5800. doi:10.1021/acs.jpcc.0c02731
- Rowe BRC, Sheskey PJ, Cook WG, Quinn ME. Handbook of pharmaceutical excipients – 7th edition. *Pharm Dev Technol*. 2013;18 (2):544. doi:10.3109/10837450.2012.751408
- Nagachinta S, Bouzo BL, Vázquez-Ríos AJ, Lopez R, de la Fuente M. Sphingomyelin-based nanosystems (SNs) for the development of anticancer miRNA therapeutics. *Pharmaceutics*. 2020;12 (2):189. doi:10.3390/pharmaceutics12020189
- Nagachinta S, Becker G, Dammico S, et al. Radiolabelling of lipid-based nanocarriers with fluorine-18 for in vivo tracking by PET. *Colloids Surf B Biointerfaces*. 2020;188:110793. doi:10.1016/j.colsurfb.2020.110793
- Ščasnar V, van Lier JE. The use of SEP-PAK SI cartridges for the preparation of gallium chloride from the citrate solution. *Eur J Nucl Med*. 1993;20(3):273. doi:10.1007/BF00170012
- Stockhofe K, Postema JM, Schieferstein H, Ross TL. Radiolabeling of nanoparticles and polymers for PET imaging. *Pharmaceutics*. 2014;7(4):392–418. doi:10.3390/ph7040392

27. Seo JW, Ang JC, Mahakian LM, et al. Self-assembled 20-nm64Cu-micelles enhance accumulation in rat glioblastoma. *J Control Release*. 2015;220:51–60. doi:10.1016/j.jconrel.2015.09.057
28. Wong P, Li L, Chea J, et al. PET imaging of 64Cu-DOTA-scFv-anti-PSMA lipid nanoparticles (LNPs): enhanced tumor targeting over anti-PSMA scFv or untargeted LNPs. *Nucl Med Biol*. 2017;47:62–68. doi:10.1016/j.nucmedbio.2017.01.004
29. Kurihara K, Ueda M, Hara I, Ozeki E, Togashi K, Kimura S. Polymeric micelle of a3 b-type lactosome as a vehicle for targeting meningeal dissemination. *Nanomaterials*. 2018;8(2):1–9. doi:10.3390/nano8020079
30. Yang BY, Moon S-H, Seelam SR, et al. Development of a multimodal imaging probe by encapsulating iron oxide nanoparticles with functionalized amphiphiles for lymph node imaging. *Nanomedicine*. 2015;10(12):1899–1910. doi:10.2217/nmm.15.41
31. Seo HJ, Nam SH, Im HJ, et al. Rapid hepatobiliary excretion of micelle-encapsulated/radiolabeled upconverting nanoparticles as an integrated form. *Sci Rep*. 2015;5:1–12. doi:10.1038/srep15685
32. Lee YK, Jeong J, Hoigebazar L, et al. Facile preparation of multimodal QDs using specially designed amphiphiles for targeting angiogenesis. *J Nucl Med*. 2011;52(supplement 1):295.
33. Helbok A, Decristoforo C, Dobrozemsky G, et al. Radiolabeling of lipid-based nanoparticles for diagnostics and therapeutic applications: a comparison using different radiometals. *J Liposome Res*. 2010;20(3):219–227. doi:10.3109/08982100903311812
34. de Arcocha-torres M, Quincoces G, Martínez-López AL, et al. Preparation, radiolabeling with 99mTc and 67Ga and biodistribution studies of albumin nanoparticles coated with polymers. *Rev Esp Med Nucl Imagen Mol*. 2020;39(4):225–232. doi:10.1016/j.remnie.2020.04.002
35. Drude N, Singh S, Winz OH, Möller M, Mottaghy FM, Morgenroth A. Multistage passive and active delivery of radiolabeled nanogels for superior tumor penetration efficiency. *Biomacromolecules*. 2017;18(8):2489–2498. doi:10.1021/acs.biomac.7b00629
36. Fernández-Barahona I, Muñoz-Hernando M, Pellico J, Ruiz-Cabello J, Herranz F. Molecular imaging with 68Ga radio-nanomaterials: shedding light on nanoparticles. *Appl Sci*. 2018;8(7):1098. doi:10.3390/app8071098
37. Malinge J, Géraudie B, Savel P, et al. Liposomes for PET and MR imaging and for dual targeting (magnetic field/glucose moiety): synthesis, properties, and in vivo studies. *Mol Pharm*. 2017;14(2):406–414. doi:10.1021/acs.molpharmaceut.6b00794
38. Ghai A, Singh B, Hazari PP, et al. Radiolabeling optimization and characterization of 68 Ga labeled DOTA–polyamido-amine dendrimer conjugate – animal biodistribution and PET imaging results. *Appl Radiat Isot*. 2015;105:40–46. doi:10.1016/j.apradiso.2015.07.021
39. Singh S, Bingöl B, Morgenroth A, Mottaghy FM, Möller M, Schmaljohann J. Radiolabeled nanogels for nuclear molecular imaging. *Macromol Rapid Commun*. 2013;34(7):562–567. doi:10.1002/marc.201200744
40. Körhegyi Z, Rózsa D, Hajdu I, et al. Synthesis of 68Ga-labeled biopolymer-based nanoparticle imaging agents for positron-emission tomography. *Anticancer Res*. 2019;39(5):2415–2427. doi:10.21873/anticancer.13359
41. Mandiwana V, Kalombo L, Hayeshi R, Zeevaart JR, Ebenhan T. Preclinical assessment addressing intravenous administration of a [68Ga]Ga-PSMA-617 microemulsion: acute in vivo toxicity, tolerability, PET imaging, and biodistribution. *Molecules*. 2021;26(9):2650. doi:10.3390/molecules26092650
42. Hübner R, Cheng X, Wängler B, Wängler C. Functional hybrid molecules for the visualization of cancer: PESIN-homodimers combined with multimodal molecular imaging probes for positron emission tomography and optical imaging: suited for tracking of GRPR-positive malignant tissue. *Chem a Eur J*. 2020;26(69):16349–16356. doi:10.1002/chem.202002386
43. Anderson CJ, Rocque PA, Weinheimer CJ, Welch MJ. Evaluation of copper-labeled bifunctional chelate-albumin conjugates for blood pool imaging. *Nucl Med Biol*. 1993;20(4):461–467. doi:10.1016/0969-8051(93)90077-8
44. Mitchell N, Kalber TL, Cooper MS, et al. Incorporation of paramagnetic, fluorescent and PET/SPECT contrast agents into liposomes for multimodal imaging. *Biomaterials*. 2013;34(4):1179–1192. doi:10.1016/j.biomaterials.2012.09.070
45. Lin M, Pallio V, Ta R, Santos EB, Ravizzini GC, Le D. What's new for 68Ga in the world of molecular imaging? *SOJ Pharm Pharm Sci*. 2018;5(4):1–12. doi:10.15226/2374-6866/5/4/00191
46. Benito AB, Aiertza MK, Marradi M, et al. Functional single-chain polymer nanoparticles: targeting and imaging pancreatic tumors in vivo. *Biomacromolecules*. 2016;17(10):3213–3221. doi:10.1021/acs.biomac.6b00941
47. Kumar V, Boddeti DK. 68Ga-radiopharmaceuticals for PET imaging of infection and inflammation. In: Baum RP, Rösch F, editors. *Theranostics, Gallium-68, and Other Radionuclides*. Springer; 2013:189–219. doi:10.1007/978-3-642-27994-2_11
48. Zhao Z, Ukidve A, Krishnan V, Mitragotri S. Effect of physicochemical and surface properties on in vivo fate of drug nanocarriers. *Adv Drug Deliv Rev*. 2019;143:3–21. doi:10.1016/j.addr.2019.01.002
49. Han X, Xu K, Taratula O, Farsad K. Applications of nanoparticles in biomedical imaging. *Nanoscale*. 2019;11(3):799–819. doi:10.1039/c8nr07769j
50. Abbina S, Parambath A. *PEGylation and Its Alternatives: A Summary*. Elsevier Ltd; 2018. doi:10.1016/B978-0-08-101750-0.00014-3
51. Zhou M, Hou J, Zhong Z, Hao N, Lin Y, Li C. Targeted delivery of hyaluronic acid-coated solid lipid nanoparticles for rheumatoid arthritis therapy. *Drug Deliv*. 2018;25(1):716–722. doi:10.1080/10717544.2018.1447050
52. Ji P, Wang L, Chen Y, Wang S, Wu Z, Qi X. Hyaluronic acid hydrophilic surface rehabilitating curcumin nanocrystals for targeted breast cancer treatment with prolonged biodistribution. *Biomater Sci*. 2020;8(1):462–472. doi:10.1039/C9BM01605H
53. Cheng Y, Liu M, Hu H, Liu D, Zhou S. Development, optimization, and characterization of PEGylated nanoemulsion of prostaglandin E1 for long circulation. *AAPS PharmSciTech*. 2016;17(2):409–417. doi:10.1208/s12249-015-0366-1
54. Hak S, Garaiova Z, Olsen LT, Nilsen AM, De Lange Davies C. The effects of oil-in-water nanoemulsion polyethylene glycol surface density on intracellular stability, pharmacokinetics, and biodistribution in tumor bearing mice. *Pharm Res*. 2015;32(4):1475–1485. doi:10.1007/s11095-014-1553-6
55. Kim K, Choi H, Choi ES, Park MH, Ryu JH. Hyaluronic acid-coated nanomedicine for targeted cancer therapy. *Pharmaceutics*. 2019;11(7):1–22. doi:10.3390/pharmaceutics11070301
56. Teijeiro-Valiño C, Novoa-Carballal R, Borrajo E, et al. A multifunctional drug nanocarrier for efficient anticancer therapy. *J Control Release*. 2019;294:154–164. doi:10.1016/j.jconrel.2018.12.002

International Journal of Nanomedicine

Dovepress

Publish your work in this journal

The International Journal of Nanomedicine is an international, peer-reviewed journal focusing on the application of nanotechnology in diagnostics, therapeutics, and drug delivery systems throughout the biomedical field. This journal is indexed on PubMed Central, MedLine, CAS, SciSearch[®], Current Contents[®]/Clinical Medicine,

Journal Citation Reports/Science Edition, EMBase, Scopus and the Elsevier Bibliographic databases. The manuscript management system is completely online and includes a very quick and fair peer-review system, which is all easy to use. Visit <http://www.dovepress.com/testimonials.php> to read real quotes from published authors.

Submit your manuscript here: <https://www.dovepress.com/international-journal-of-nanomedicine-journal>